CrystEngComm

Accepted Manuscript

This article can be cited before page numbers have been issued, to do this please use: H. Perez, A. Di Santo, O. E. Piro, G. A. Echeverría, A. Cano, M. González M., J. Rodríguez-Hernández, A. Ben Altabef, A. Frontera and D. M. Gil, *CrystEngComm*, 2020, DOI: 10.1039/D0CE01596B.

ROYAL SOCIETY OF CHEMISTRY

rsc.li/crystengcomm

View Article Online
DOI: 10.1039/D0CE01596B

ARTICLE

A first exploration of isostructurality in transition metal nitroprussides: X-ray analysis, magnetic properties and DFT calculations

Received 00th January 20xx,
Accepted 00th January 20xx

DOI: 10.1039/x0xx00000x

Hiram Pérez[a,*], Alejandro Di Santo[b], Oscar E. Piro[c,d], Gustavo A. Echeverría[c,d], A. Cano[e], M. González[e], J. Rodríguez-Hernández[f], A. Ben Altabef[b,d], Antonio Frontera[g,*] and Diego M. Gil[h,d*]

Five new transition metal nitroprussides with 1-methylimidazole (1-MeIm)] have been synthesized and characterized by IR, XPS and UV-Vis spectroscopies, thermal analysis, and powder and single-crystal X-ray diffraction. The structural analyses have revealed that the complexes $Mn(1\text{-MeIm})_2[Fe(CN)_5NO]$ (**1**), $Fe(1\text{-MeIm})_2[Fe(CN)_5NO]$ (**2**), $Cu(1\text{-MeIm})_4[Fe(CN)_5NO]$ (**3**), $Zn(1\text{-MeIm})_2[Fe(CN)_5NO]$ (**4**) and $Cd(1\text{-MeIm})_2[Fe(CN)_5NO]$ (**5**) are 2D coordination polymers. The supramolecular self-assembly for all the five complexes is governed by non-classical C-H···N hydrogen bonds and lone-pair(O)···π interactions. N···O chalcogen and π···π contacts are also present in the crystal packing of the complexes **1**, **2**, **4** and **5.** A detailed analysis of four geometric descriptors revealed the existence of a high degree of isostructurality for the molecular pair **1**/**2**, and a moderate one for the pairs **1**/**5** and **2**/**5**. The *dissimilarity index* was also calculated for molecular pairs in two series of related compounds, showing that the degree of similarity is lower than those found in the pairs **1**/**2**, **1**/**5** and **2**/**5**. The results herein discussed for first time in the literature may be useful to understand property/structure relationships in these types of complexes. By using DFT calculations at the PBE0-D3/def2-TZVP level of theory and discrete models of the coordination polymers, we have analyzed cooperative lp–π/π–π/π–lp assemblies that are observed in the solid state of these compounds. This interesting assembly has been further analyzed by a combination of QTAIM, NCIplot and MEP surface calculations. The magnetic measurements indicate that compounds **1–3** are paramagnetic at 300 K and the Curie-Weiss constants are negative suggesting weak antiferromagnetic coupling between the metal centers, at very low temperatures.

Introduction

Metal-organic compounds, including hybrid inorganic-organic solids have attracted intense interest due to their structural diversities and interesting potential applications, such as molecular sensors,[1] heterogeneous catalysis,[2] magnetic materials,[3] non-linear optical activity,[4] and electrical conductivity.[5] These coordination compounds have advantages over organic compounds with regards to the formation of molecular building blocks, because metal ions show a great variety of coordination geometries and also a wide range of physical properties.[6] One of the basic strategies in crystal engineering is the preparation of compounds with the desired physical properties, for which structure-property relationships should be investigated.[7–11]

Layered transition metal nitroprussides are 2D coordination polymers in which the axial coordination sites for the metal coordinated to the N ends of equatorial CN ligands are available to form a chemical bond with organic molecules containing basic terminal groups.[12–18] The intercalation process produces solids with 3D structure, where the intercalated molecules interact with neighboring layers through different intermolecular interactions, including hydrogen and weak π···π stacking bonds. These contacts also provide electron communication paths involving the metal centers, which give rise to the observed magnetic properties of those compounds.[12–18] Recently, the intercalation of pyridine derivatives to ferrous nitroprusside produced systems with small structural changes showing thermally-induced spin transitions.[17,18] The two spin states and the transition between them were characterized by magnetic, DSC and Raman measurements.

A common structural feature in various series of transition metal nitroprussides previously reported[12–15] is the presence of compounds with similar lattice parameters and space

[a.] *Departamento de Química General e Inorgánica, Facultad de Química, Universidad de La Habana, CP 10400, La Habana, Cuba. alinaca@infomed.sld.cu*
[b.] *INQUINOA (CONICET – UNT). Instituto de Química Física. Facultad de Bioquímica, Química y Farmacia. Universidad Nacional de Tucumán. San Lorenzo 456. T4000CAN. San Miguel de Tucumán. Argentina.*
[c.] *Departamento de Física, Facultad de Ciencias Exactas, Universidad Nacional de La Plata and IFLP institute (CONICET, CCT-La Plata). C.C. 67, 1900, La Plata. Argentina.*
[d.] *Members of the Research Career of CONICET*
[e.] *Instituto Politécnico Nacional, Centro de Investigación en Ciencia Aplicada y Tecnología Avanzada, U. Legaria, Ciudad de México, México.*
[f.] *Centro de Investigación en Química Aplicada (CIQA), Blvd. Enrique Reyna Hermosillo Nº 140, Saltillo, Coahuila 25294, México.*
[g.] *Departament de Química, Universitat de les Illes Balears, Crta de Valldemossa km 7.5, 07122 Palma de Mallorca (Baleares), SPAIN. toni.frontera@uib.es*
[h.] *INBIOFAL (CONICET – UNT). Instituto de Química Orgánica. Facultad de Bioquímica, Química y Farmacia. Universidad Nacional de Tucumán. Ayacucho 471. T4000INI. San Miguel de Tucumán. Argentina. diego.gil@fbqf.unt.edu.ar*

† Electronic Supplementary Information (ESI) available: XRD patterns, additional Figures showing X-ray packing, IR spectra, TG and DTA curves, magnetic curves, X-ray measurement details and Tables S1 to S6. See DOI: 10.1039/x0xx00000x

symmetry. However, a complete description of the important phenomenon of isostructurality has not been the main goal in those papers. The IUCr has defined that ''two crystals are said to be isostructural if they have the same crystal structure, but not necessarily the same cell dimensions nor the same chemical composition''. Diverse descriptors have been defined to calculate the degree of similarity between two structures. In addition to the existence of similar axial ratios and inter-axial angles, the variation of the lattice parameters can be estimated, as well as the distance differences between the crystal coordinates of identical non-H atoms within the same section of the asymmetric unit of the related *(A* and *B)* structures.[9] Other measure of similarity has been described as a function of the differences in atomic positions (weighted by the multiplicities of the sites) and the ratios of the corresponding structure lattice parameters.[10] A more recent and versatile procedure for the identification, visualization and quantification of structural similarity in organic crystals, mixed component crystals, and polymeric structures has been reported,[11] considering not only geometric aspects but also packing effects.

We report here a novel series of five inorganic-organic hybrid solids obtained by intercalation of 1-metilimidazole (1-MeIm) in transition metal nitroprussides. The compounds were characterized by IR, XPS and UV-Vis spectroscopies as well through thermogravimetric (TG) and differential thermal (DT) analysis. In addition, the magnetic properties of compounds **1-3** were described in detail.

Crystal structures were solved by single-crystal X-ray diffraction (XRD) for Mn(II), Cu(II), Zn(II) and Cd(II) complexes, and by powder XRD for Fe(II) complex. For the first time in this type of compounds, in an effort for exploring the degree of structural similarity, we have computed various descriptors of isostructurality in molecular pairs of the new series of complexes and the results are compared to those of two series of related compounds. Finally, using discrete models we have analyzed the formation of lp–π/π–π/π–lp assemblies in the solid state involving the π-system of the 1-methylimidazole and the lone pair of the O-atom of the nitrosyl ligand, focusing on the influence of the lp–π interaction on the π-stacking.

Experimental

Materials and instrumentation

All reagents and solvents employed for the synthetic process were used as received, without further purification. Elemental analysis for carbon, hydrogen and nitrogen was performed using a Carlo Erba EA1108 analyzer. The IR absorption spectra were recorded in the solid state using KBr pellets on a FTIR Perkin Elmer GX1 spectrometer in the 4000-400 cm^{-1} frequency range, with 4 cm^{-1} spectral resolution. Diffuse reflectance UV-Vis spectra of complexes were measured using a Shimadzu UV-2600 spectrophotometer equipped with an integrating sphere and employing $BaSO_4$ as reference. TG and DTA curves were measured with a Shimadzu DTG-50 thermo-balance in the 25-800 ºC range at a heating rate of 5 ºC/min under air flow. The XPS spectra were recorded with an electron spectrometer model K-alpha+ from Thermo Scientific Co. The instrument is equipped with a monochromatic Al Kα source (1486.8 eV), electron gun and Argon ion source. The electron detector is an electrostatic hemispherical analyzer (HAS) set up to constant analyzer transmission (CAT) mode, where Δ*E*= constant. The measurements were carried out under standard conditions, room temperature and the base pressure in the analysis chamber was maintained at 2 x 10^{-9} mBar. The X-ray spot size chosen was 400 µm. During the experiment, the electron gun was used to minimize the effects of the positive surface charging as result of the photoelectrons ejection. The powder samples were homogeneously pressed on conductor carbon double-side tape attached on a stain steel sample holder. For elemental analysis purposes, the survey spectra were recorded with a pass energy of 160 eV and 0.5 eV step size. For the high-resolution spectra, the pass energy and step size were set up at 20 eV and 0.1 eV. The core-level regions were analyzed with the Avantage v5.9919 software provided by the spectrometer manufacturer. The spectra were fitted using Gaussian-Lorentzian (70:30) curves, the background was calculated and subtracted using the Shirley baseline model. The chemical composition was calculated considering a homogeneous distribution of atoms in a selected area. The zero-field cooling (ZFC) and field cooling (FC) curves were collected from 2-300 K, under an applied field of 50 Oe, using a MPMS-3 magnetometer from Quantum Design. The effective magnetic moment (M_{eff}) was calculated according to M_{eff} = 2.828sqrt(χ_MT), considering the diamagnetic contribution in accordance to Pascal constant for the involved atoms.

Preparation of $[M(1\text{-}MeIm)_2[Fe(CN)_5NO]$ (M: Mn^{2+}, Fe^{2+}, Cu^{2+}, Zn^{2+}, Cd^{2+}) (1-5)

The series of complexes **1**-**5** were obtained by a co-precipitation method, by mixing aqueous solutions of $Na_2[Fe(CN)_5NO]\cdot 2H_2O$ (1 mmol), 1-MeIm (2 mmol) and MCl_2 (M: Mn^{2+}, Zn^{2+}) and $CdBr_2$ and $Fe(NH_4)_2(SO_4)_2$ for complexes **5** and **2**, respectively. To prevent the oxidation of Fe(II), we added ascorbic acid to the solution. The complex **3** was obtained by a similar method used for the other compounds, except that in this case DMF was used as solvent. The fine solids formed were kept for a week in the refrigerator, and then separated by filtration and washed several times with distilled water to remove the unreacted salts. The solids were stored in the dark in a desiccator over $CaCl_2$ and the nature of the formed compounds was assessed by elemental analysis, IR and TGA-DTA data.

Single crystals adequate for structural X-ray diffraction were obtained for **1**, **3-5** compounds by a slow diffusion technique. One side of an H-shaped vessel contains a mixture of MCl_2 (M: Mn, Cu, Zn and Cd) in water. The other side contains an ethanol-water solution (1:1) of 1-methylimidazole and $Na_2[Fe(CN)_5NO]$. Crystals of the compounds were obtained after a period of 20 days.

$Mn(1\text{-}MeIm)_2[Fe(CN)_5NO]$ (**1**): Yellow powder. Yield: 80%. Anal. Calcd. for $MnFeC_{13}H_{12}N_{10}O$: C, 35.9; H, 2.8; N, 32.2%. Found: C, 34.8; H, 2.7; N, 31.9%.

$Fe(1\text{-}MeIm)_2[Fe(CN)_5NO]$ (**2**): Red powder. Yield: 60%. Anal.

Calcd. for $Fe_2C_{13}H_{12}N_{10}O$: C, 35.8; H, 2.8; N, 32.1%. Found: C, 35.6; H, 2.8; N, 32.1%.

$Cu(1\text{-}MeIm)_4[Fe(CN)_5NO]$ (**3**): Blue powder. Yield: 85%. Anal. Calcd. for $CuFeC_{21}H_{24}N_{14}O$: C, 41.5; H, 4.0; N, 32.8%. Found: C, 41.8; H, 4.2; N, 33.0%.

$Zn(1\text{-}MeIm)_2[Fe(CN)_5NO]$ (**4**): Pink powder. Yield: 90%. Anal. Calcd. for $ZnFeC_{13}H_{12}N_{10}O$: C, 35.0; H, 2.7; N, 31.4%. Found: C, 34.8; H, 2.7; N, 31.2%.

$Cd(1\text{-}MeIm)_2[Fe(CN)_5NO]$ (**5**): Pink powder. Yield: 75%. Anal. Calcd. for $CdFeC_{13}H_{12}N_{10}O$: C, 31.7; H, 2.6; N, 28.4%. Found: C, 31.9; H, 2.7; N, 28.2%.

Single crystal X-ray diffraction data

The measurements were performed on an Oxford Xcalibur, Eos, Gemini CCD diffractometer employing graphite-monochromated MoKα (λ = 0.71073 Å) radiation. X-ray diffraction intensities were collected (ω scans with ϑ and κ-offsets), integrated and scaled with CrysAlisPro[19] suite of programs. The unit cell parameters were obtained by least-squares refinement (based on the angular settings for all collected reflections with intensities larger than seven times the standard deviation of measurement errors) using CrysAlisPro. Data were corrected empirically for absorption employing the multi-scan method implemented in CrysAlisPro. The structures were solved by the intrinsic phasing procedure implemented in SHELXT[20] and the corresponding non-H molecular model refined with anisotropic displacement parameters with SHELXL.[21]

$Mn(1\text{-}MeIm)_2[Fe(CN)_5NO]$: The manganese complex is isomorphic to the cadmium counterpart, namely $Cd(1MeIm)_2[Fe(CN)_5NO]$. The agreement R1-value of the non-H molecular model was 0.1071 and the maximum residual electron density Δρ = 4.78 e.Å^{-3}, somewhat large values in part because of distortion of diffraction intensities due to overlapping with the ones of a second crystal domain (of about 34% scattering power) that integrates the sample and it is rotated in about 180º around the reciprocal ***a****-axis of the dominant domain (twin). After elimination from the data set those reflections having a degree of overlapping higher than 80% with the second largest domain in the sample, the R1 and Δρ values drooped to 0.046 and 1.17 e.Å^{-3}, respectively.

The hydrogen atoms were positioned at their expected geometrical locations and refined with the riding model. The methyl H-atom positions were optimized by treating them as

Table 1. Crystallographic data and structure refinement results for **1-5**

	1	**2**[b]	**3**	**4**	**5**
Empirical formula	$C_{13}H_{12}FeMnN_{10}O$	$C_{13}H_{12}Fe_2N_{10}O$	$C_{21}H_{24}FeCuN_{14}O$	$C_{13}H_{12}FeZnN_{10}O$	$C_{13}H_{12}FeCdN_{10}O$
Formula weight	435.12	436.0	607.93	445.55	492.58
Temperature (K)	297	298	297	297	297
Wavelength (Å)	0.71073	1.54056	0.71073	0.71073	0.71073
Crystal system	Monoclinic	Monoclinic	Triclinic	Orthorhombic	Monoclinic
Space group	$P2_1/c$	$P2_1/c$	$P\bar{1}$	$Pbca$	$P2_1/c$
Unit cell parameters					
a (Å)	8.4311(10)	8.386(2)	9.1670(5)	14.8493(11)	8.4002(3)
b (Å)	14.9364(15)	14.787(4)	10.2296(5)	14.4980(10)	15.2133(5)
c (Å)	14.6337(16)	14.458(3)	15.6179(8)	16.5461(12)	14.8960(5)
α (º)	90.0	90.0	73.752(4)	90.0	90.0
β (º)	97.228(11)	96.9(1)	80.350(4)	90.0	98.048(3)
γ (º)	90.0	90.0	84.476(4)	90.0	90.0
Volume (Å^3)	1828.2(4)	1779.86	1383.3(1)	3562.1(4)	1884.9(1)
Z	4	4	2	8	4
ρ calc. (mg mm^{-3})	1.581	1.582	1.459	1.662	1.736
μ (mm^{-1})	1.509	-	1.334	2.186	1.922
F(000)	876	-	622	1792	968
Crystal size (mm^3)	0.037 x 0.112 x 0.223	-	0.058 x 0.122 x 0.338	0.059 x 0.108 x 0.122	0.062 x 0.143 x 0.202
ϑ-range (º)	2.983-25.985	2-30	2.965-26.499	2.810-25.994	2.958-25.993
Index ranges	-10 ≤ h ≤ 10	-5 ≤ h ≤ 5	-11 ≤ h ≤ 11	-17 ≤ h ≤ 12	-10 ≤ h ≤ 9
	-18 ≤ k ≤ 17	0 ≤ k ≤ 9	-12 ≤ k ≤ 12	-11 ≤ k ≤ 17	-18 ≤ k ≤ 12
	-17 ≤ l ≤ 18	0 ≤ l ≤ 9	-19 ≤ l ≤ 19	-20 ≤ l ≤ 19	-13 ≤ l ≤ 18
Reflections collected	8308	634	11398	7971	7780
Unique reflections	2866	512	5585	2946	3693
R(int)	0.0783	-	0.0290	0.0883	0.0357
Parameters/Restrains	240/0	46/22	350/0	237/0	240/0
Goodness-of-fit on F^2	0.813	2.80	1.010	0.762	1.033
R[a] indices [I>2σ(I)]	R1= 0.0460	R1= 10.6	R_1 = 0.0397	R_1= 0.0492	R_1 = 0.0387
	wR2 = 0.0940	-	wR_2 = 0.0828	wR_2 = 0.0928	wR_2 = 0.0818
R indexes (all data)	R1 = 0.1037	R1= 17.8	R_1= 0.0611	R_1= 0.1220	R_1 = 0.0670
	wR2 = 0.1942	-	wR_2 = 0.0938	wR_2 = 0.1048	wR_2 = 0.0974
Δρ (e Å^{-3})	1.175, -0.700		0.312, -0.513	1.301, -0.601	0.722, -0.602
CCDC	2014751	2013009	2014754	2014752	2014753

[a]$R_1=\Sigma||F_o|-|F_c||/\Sigma|F_o|$, $wR_2=[\Sigma w(|F_o|^2-|F_c|^2)^2/\Sigma w(|F_o|^2)^2]^{1/2}$; [b]Data blanks correspond to parameters not related to powder XRD.

rigid groups allowed to rotate during the refinement around the corresponding N-CH_3 bonds such as to maximize the sum of the residual electron density at the calculated H-positions.

Cu(1-MeIm)$_4$[Fe(CN)$_5$NO]: The H-atoms were refined as for Mn(1-MeIm)$_2$[Fe(CN)$_5$NO].

Zn(1-MeIm)$_2$[Fe(CN)$_5$NO]: The H-atoms were refined as for Mn(1-MeIm)$_2$[Fe(CN)$_5$NO]. At this stage, the R_1-value is 0.0624 and the maximum residual electron density Δρ equal to = 2.13 e.Å^{-3}. These values are somewhat large in part because of distortion of diffraction intensities due to overlapping with the ones of a second crystal domain (of about 23% scattering power) that integrates the sample and it is rotated in about 180º around the reciprocal **a***-axis of the dominant domain (twin). After elimination from the data set those reflections having a degree of overlapping higher than 80% with the second largest domain in the sample, the R_1 and Δρ values drooped to 0.0491 and 1.30 e.Å^{-3}, respectively.

Cd(1-MeIm)$_2$[Fe(CN)$_5$NO]: Isomorphic to Mn(1-MeIm)$_2$[Fe(CN)$_5$NO]. The H-atoms were refined as for Mn(1MeIm)$_2$[Fe(CN)$_5$NO].

Powder XRD data

The powder X-ray diffraction pattern was collected using a Bragg-Brentano geometry with CuKα1 radiation (λ = 1.54056 Å) in a PANalytical X'per Pro diffractometer with detector linear Pixcel 1D. Diffraction data was recorded from 4 to 60° (2θ) at a step size of 0.02° and 10 s of counting time. The sample was ground in an agate mortar and the loose powder pressed into the diffractometer sample holder. The structural refinement against the powder XRD pattern was performed by the Rietveld method implemented in the FULLPROF program and using as structural model the crystal structure of the isomorphic complex **1**.[23] The cell parameters and peak profiles were refined using the Le Bail pattern fitting method[24] with pseudo-Voigt peak shape functions. The background was modeled by a third-order polynomial fitting.

The final refinement was carried out on all atomic parameters. Restrictions were applied to interatomic distances within the pentacyanonitrosyl anion and methylimidazole ring. Refinement procedure, refined atomic positions, thermal and occupation factors, as well as bond lengths and angles are available in Tables S1-S2, ESI**.**

Crystal data and structure refinement results for complexes **1**-**5** are summarized in Table 1. Molecular and packing graphics were prepared with Mercury software.[25] Crystallographic structural data have been deposited with the Cambridge Crystallographic Data Centre (CCDC). Enquires for data can be direct to Cambridge Crystallographic Data Centre, 12 Union Road, Cambridge, UK, CB2 1EZ or by e-mail to deposit@ccdc.cam.ac.uk or fax to +44(0)1223 336033. Any request to CCDC for this material should quote the full literature citation and the reference number CCDC 2014751 (**1**), 2013009 (**2**), 2014754 (**3**), 2014752 (**4**), 2014753 (**5**).

Description of isostructurality

Comparison, superposition and visualization of molecules for pairs of complexes were carried out with Olex2 (version 1.2.7).[22]

The procedure find relation between the connectivity graphs of molecular fragments of loaded structures aligns the selected fragments and prints corresponding root mean square distances (RMSD). Four geometric descriptors of isostructurality were computed:

(1) *unit-cell similarity index* Π,[9] based on axial ratios, given values almost zero for cases of great similarity.

(2) *isostructurality index* $I_i(n)$ (in %),[9] based on distance differences between the crystal coordinates of identical non-H atoms, the larger percentages being associated to higher isostructurality.

(3) *measure of similarity* Δ[10] based on weighted mean differences of atomic coordinates, along with relations between the axial ratios.

(4) *dissimilarity index* '*X*'[11] by using of Xpac2.0.2,[11a] a software that compares representative lists of internal coordinates-distances, intermolecular angles, dihedral angles and torsion angles. The Xpac method allows the identification of similar packing arrangements present between two crystal structures.[11b] The basic geometrical features of any molecule can be described by an ordered set (OSP) formed by a suitable selection of *n* atoms ($n \geq 3$). A second ordered set may describe a second molecule with the same or a similar structure. If both sets represent two similar arrangements of points in the same order, then we regard them as corresponding ordered sets of points (COSP). Common structural motifs present in crystal structures to be compared are termed as 'supramolecular constructs' (SCs), which represent sub-components of complete crystal structures). The SC may be 0D similarity, 1D similarity (row of molecules match), 2D similarity (layer of molecules match) and 3D similarity (isostructural). Xpac defines the dissimilarity index '*X*' as a measure of how far the two crystal structures deviate from perfect geometrical similarity.[11c,d] The lowest value for *X* indicates the highest degree of similarity. *X* values smaller than 1º are found for SCs with high similarity, whereas SCs of low-degree similarity produce *X* values of 6ᵘ or even higher. Stretch parameter D (in Å), as well as the delta(a)/delta(p) and *X*/delta(d) plots (a = angular deviation, p = interplanar angular deviation, d = molecular centroid distance deviation) in the results window will also give an indication of the appropriate level for these parameters.

Theoretical methods

The energies of the complexes and compounds studied herein were computed at the PBE0[26]-D3[27]/def2-TZVP[28] level of theory using the Gaussian-16 program.[29] The Bader's "Atoms in molecules" theory and NCI method[30] calculations were carried out using the AIMall calculation package.[31] The interaction energies have been BSSE corrected by using the counterpoise method.[32] The MEP surfaces were plotted using the 0.001 iso-surface and the NCIplot ones using the 0.5 a.u. iso-surface. The cut-off used for the NCIplot was ρ = 0.03 a.u. The PBE0-D3 level of theory has been recently used by us to analyze a variety of noncovalent interactions in the solid state.[33–35]

Results and discussion

Crystal structure description of complexes 1-5.

The crystal structures of all the five complexes are polymeric. Complexes **1, 2** and **5** are essentially isomorphic to one another, and crystallize in the monoclinic space group $P2_1/c$ with Z = 4 molecules per unit cell. The complex **3** crystallizes in the triclinic SG $P\bar{1}$ with Z = 2, whereas the complex **4** crystallizes in the orthorhombic SG *Pbca* with Z= 8. Selected bond lengths and angles around the metal centers are listed in Table S3, ESI. Due to difficulties to growth suitable single crystals, the structure of **2** was solved by powder X-ray diffraction, and refined using the data of complex **1** as a structural model. The experimental and the best fitted calculated powder XRD patterns are compared in Fig. S1, ESI.

The coordination environments of the M(II) ions for complexes **1**, **3** and **4** are respectively depicted in Figs. 1a, 2a and 3a. Analogous stereochemistry geometry to the one of **1** is shown in Figs. S2a and S3a for complexes **2** and **5**, respectively. In complexes **1**, **2**, **4** and **5**, the metal center M is octahedral coordinated to four N atoms from the CN ligands [M-N bond lengths in the range 2.2198(6)-2.4094(1) Å] and its axial coordination sites are occupied by two N atoms from the 1-MeIm ligands [M-N distances in the range 2.2178(6)-2.2844(1) Å]. In complex **3**, the Cu(II) ion is in a quite regular octahedral environment, equatorially coordinated to four 1-MeIm ligands through their N-atoms and to the N atoms of two cyanide ligands. The Cu(II) and Fe(II) metal centers are connected through a CN bridge.

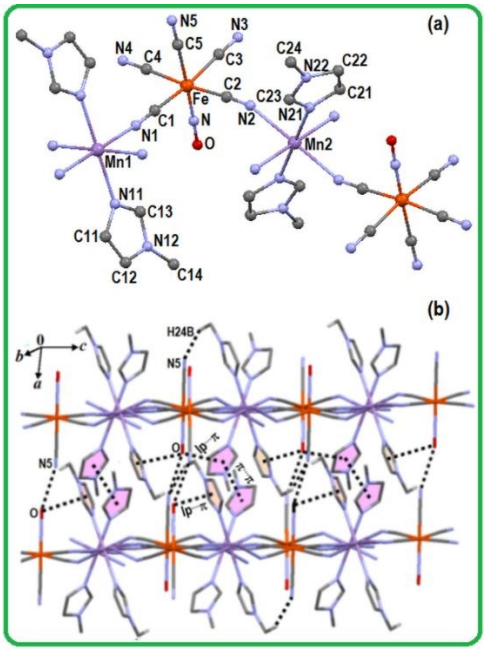

Fig. 1. (a) Coordination environment of Mn(II) and Fe(II) ions in complex **1** showing the atom numbering scheme. H-atoms are omitted for clarity (b). View of the crystal packing depicting C-H···N hydrogen bond, chalcogen O···N5, π···π and lone-pair(O)···π interactions.

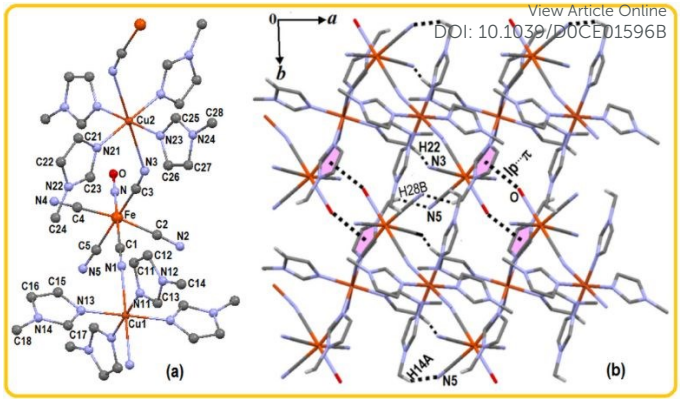

Fig. 2. (a) Coordination environment of the Cu(II) and Fe(II) ions in complex **3** showing the atom numbering scheme. H-atoms are omitted for clarity (b). View of the crystal packing depicting C-H···N hydrogen bonds and lone-pair(O)···π interactions.

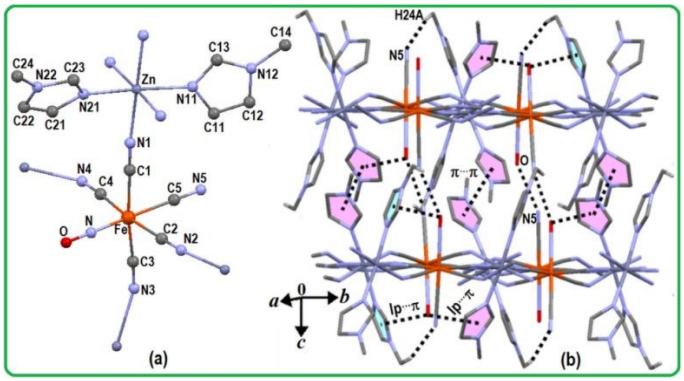

Fig. 3. (a) Coordination environment of the Zn(II) and Fe(II) ions in complex **4** showing the atom numbering scheme. H-atoms are omitted for clarity (b). View of the crystal packing depicting C-H···N hydrogen bond, chalcogen O···N5, π···π and lone-pair(O)···π interactions.

As expected, the Fe(II) ion in the nitroprusside anion is six-coordinated by five carbon atoms from cyanide ligands (four cyano groups are bridged and one is terminal) and the nitrosyl N atom. Bond lengths and angles in the nitroprusside anion (Table S3, ESI) are in accordance with corresponding reported values for related complexes.[12–18] In all the compounds, the $[Fe(CN)_5NO]^{2-}$ anion exhibits the expected distorted octahedral geometry around the Fe(II) ion, as reflected by C_{eq}-Fe-NO and C_{eq}-Fe-C_{ax} angles with values greater and lower than 90º, respectively (Table S3, ESI).

Figs. 1b, 2b and 3b show a view of the crystal packing for complexes **1, 3** and **4**, respectively. The absence of H-atom coordinates in the CIF prompted us to position them, with the aim of analyzing the expected hydrogen bond interactions for complex **2**. Thus, all the H-atoms were positioned at a distance of 1.08 Å from their carbon parent using two modules (retcif and retcor) of the CLP-Pixel program package.[36] Analogous diagrams to one of **1** are shown in Figs. S2b and S3b for **2** and **5**, respectively. The crystal structure for all the five complexes is further stabilized by non-classical C-H···N hydrogen bonds (Table 2). These interactions involve donor methyl (C24) H-atoms (one for **1** and **4**, and two for **2** and **5**) of an imidazole group, acting the N4 and/or N5 atoms of cyanide ligands as acceptors. The network of C-H···N hydrogen bonds is somewhat

View Article Online
DOI: 10.1039/D0CE01596B

more extensive for **3**, participating methyl H-atoms of three imidazole groups. Further, all the C-H···N contacts in structures **1**-**5** are remarkably shorter than the sum of van der Waals radii (2.75Å), but they represent moderate hydrogen bonds[37] with H···N distances in the range 2.502-2.738 Å, and average directionality around 152°. It is worthwhile to mention that crystallographic evidence for the existence of short C-H···N hydrogen bond, as well as statistical and energetic analyses on the significant influence of this type of interaction in crystal packing has been reported.[38]

Table 2. Geometrical parameters of the H-bonding interactions for compounds **1**-**5**.

D-H···A	D-H	H···A	D···A	<(D-H···A)	symmetry
Compound **1**					
C24-H24B···N5	0.96	2.67	3.566(8)	155	x, ½-y, -½+z
Compound **2**					
C24-H24C···N4	-	-	3.59(7)	-	-1+x, ½-y, -½+z
C24-H24B···N5	-	-	3.53(7)	-	x, ½+y, -½+z
Compound **3**					
C22-H22···N3	0.93	2.55	3.312(4)	139	1-x, 1-y, 2-z
C28-H28B···N5	0.93	2.59	3.472(5)	154	-1+x, 1+y, z
C14-H14A···N5	0.93	2.50	3.403(6)	156	1-x, 1-y, 1-z
Compound **4**					
C24-H24A···N5	0.96	2.65	3.528(9)	153	1-x, ½+y, ½-z
Compound **5**					
C24-H24C···N5	0.96	2.69	3.596(7)	158	x, -y+½, z-½
C24-H24A···N4	0.96	2.74	3.646(7)	158	x-1, -y+½, z-½

Unlike structure **3**, the 3D framework is also supported by significant O···N5 chalcogen interactions in the remaining structures, as observed in related complexes.[13] The d(O···N) distances of 3.0563(3), 3.0308(1) and 2.983(7) Å for **1**, **2** and **4**, respectively, are below the sum of the van der Waals radii (3.07 Å),[19] and somewhat above [3.1084(1) Å] for complex **5.** Other structural feature in contrast with **3** is the presence of face-to-face π-stacking interactions[39] between adjacent imidazole rings in **1**, **2, 4** and **5**, with very similar inter-centroid distances [average *Cg*1···*Cg*1 = 3.449(1) Å] which also control the supramolecular self-assembly. The geometrical parameters of π···π contacts with *Cg*···*Cg* < 3.8 Å are shown in Table 3. Finally, other common characteristic in all the five structures is the appearing of short contacts between the oxygen atoms and the imidazole rings. Geometrical descriptors of these contacts are listed in Table 4. In the case of complexes **1**, **2** and **5**, the O atom is in contact with two different rings (centroids *Cg*1 and *Cg*2), whereas **3** and **4** only exhibit one contact. The O···*Cg*1 and O···Cg4 distances are shortest and close similar with average value of 3.246(1) Å (< 3.8 Å), indicating lone-pair···π (lp···π) interactions.[40,41] Moreover, the average angular distribution (deviation of the angle α from 120°, where α is the angle N-O···*Cg*) of 16.4° shows significant lp···π interactions,[40] while the average angle ω of 35.5° reveals that the nitrosyl group takes an angular approach towards the ring.

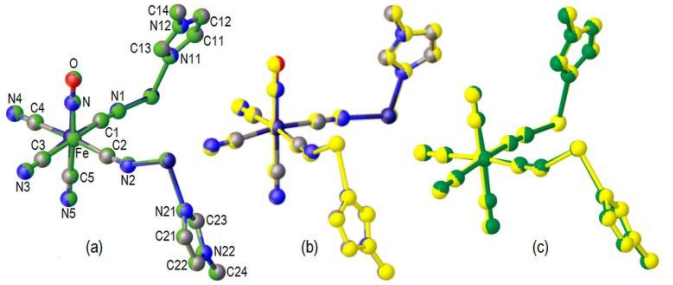

Fig. 4. Overlay diagrams of the asymmetric units for (a) **1**/**2**, (b) **1**/**5** and (c) **2**/**5** pairs of complexes. Complex **1** shows atomic identities. Complexes **2** and **5** are shown in green and yellow, respectively.

Of the five distances separating the electron-rich O atom from each atom of the ring N11/N12/C11-C13, only the O···C12 distance is below the corresponding sum of van der Waals radii (3.22 Å), with values of 3.006(9) Å, 2.97(9) Å, 2.976(9) Å and 3.018 (7) Å for complexes **1**, **2, 4** and **5**, respectively. A similar behavior is observed for complex **3**, where the short O···C27 distance of 3.195 (4) Å is lightly longer than in the remaining structures, but the absence of O···N5 chalcogen and π···π interactions increase the importance of the lp···π contact. These

Table 3. Geometrical parameters (Å,°) of π···π interactions or compounds **1**, **2, 4** and **5.**

Cg(I)···*Cg*(J)[a]	*R*c[b]	*R*1v[c]	*R*2v[d]	Slipp[e]	α[f]	β[g]	γ[h]	symmetry
Compound **1**								
*Cg*1···*Cg*1	3.4544(4)	3.3391	3.3391	0.885	0.00	14.8	14.8	2-x,1-y,1-z
Compound **2**								
*Cg*1···*Cg*1	3.4464(9)	3.3304	3.3304	0.887	0.00	14.9	14.9	2-x,1-y,1-z
*Cg*2···*Cg*2	3.7947(10)	3.7061	3.7061	0.815	0.00	12.4	12.4	-x,-y,1-z
Compound **4**								
*Cg*1···*Cg*1	3.4334(3)	3.3188	3.3188	0.879	0.00	14.8	14.8	1-x,1-y,-z
Compound **5**								
*Cg*1···*Cg*1	3.4661(1)	3.3407	3.3407	0.924	0.00	15.5	15.5	2-x,1-y,1-z

[a] *Cg*1 and *Cg*2 are the centroids of the rings N11/N12/C11-C13 and N21/N22/C21-C23, respectively. [b]Centroid distance between ring I and ring J; [c] Vertical distance from ring centroid I to ring J; [d] Vertical distance between ring centroid J to ring I; [e] Slippage = distance between *Cg*(I) and Perpendicular Projection of *Cg*(J) on Ring I; [f] Dihedral angle between mean planes I and J; [g] Angle between the centroid vector *Cg*(I)···*Cg*(J) and the normal to the plane (I); [h] Angle between the centroid vector *Cg*(I)···*Cg*(J) and the normal to the plane (J).

results reflect the existence of moderate lp···π interactions in all the compounds of the series.[42]

Analysis of isostructurality for complexes 1, 2 and 5.

Unlike the structures **3** and **4**, some degree of similarity in the unit cell parameters and the same space group for complexes **1**, **2**, and **5** (Table 1) was observed, suggesting potential existence of isostructurality. Taking into account that the 'approximate isomorphism' of molecules is a prerequisite for their similar packing,[7] we firstly have drawn overlay diagrams considering asymmetric units for molecular pairs **1/2**, **1/5** and **2/5** (**Fig. 4**). It is clearly seen that the first molecule is virtually super-imposable upon the second one, being this feature more evident in the order **1/2** > **1/5** > **2/5** as reflected by alignment RMSD (without inversion) values of 0.039, 0.073 and 0.100 Å, respectively.

Table 4. Geometry of the lone-pair(O)···π interactions for **1-5** (Å, º)

	Symm.	O···*Cg*[a]	O⊥π[b]	γ[c]	α[d]	ω[e]
		Compound **1**				
N-O···*Cg*1	x, ½-y, ½+z	3.2653(4)	2.971	24.5	103.2	37.6
N-O···*Cg*2	1-x, -y, 1-z	3.7064(4)	3.295	27.3	107.7	23.2
		Compound **2**				
N-O···*Cg*1	x, ½-y, ½+z	3.2250(9)	2.941	24.2	103.5	37.6
N-O···*Cg*2	1-x, -y, 1-z	3.6605(10)	3.247	27.5	107.2	22.7
		Compound **3**				
N-O···*Cg*4	x, -1+y, z	3.2438(2)	3.153	13.6	109.9	26.7
		Compound **4**				
N-O···*Cg*1	-½+x, y, ½-z	3.2251(2)	2.909	25.6	103.0	38.1
		Compound **5**				
N-O···*Cg*1	x, ½-y, ½+z	3.2707(1)	2.985	24.1	103.5	37.6
N-O···*Cg*2	1-x, -y, 1-z	3.7364(1)	3.378	25.3	109.8	24.4

[a]*Cg*1, *Cg*2 and *Cg*4 are the centroids of the rings N11/N12/C11-C13, N21/N22/C21-C23 and C23-C27, respectively; [b]perpendicular distance of atom O on aromatic ring plane; [c]angle between O···*Cg* vector and normal to ring plane; [d]angle N-O···*Cg*; [e]angle between the N-O bond line and the ring plane.

In order to estimate the internal motion of the lattice parameters in the complexes **1**, **2** and **5**, we have calculated the *unit-cell similarity index* Π,[8] leading to values of 0.010, 0.013 and 0.022 for **1/2**, **1/5** and **2/5**, respectively, which indicate high similarity for the three pairs. In addition, the two pairs involving manganese show uppermost and close similarity as reflected by very similar Π values twice shorter than that for the pair **2/5**. On the other side, for estimating the effect of the differences in the geometry of the molecules and the positional differences on the structural similarity, the *isostructurality index* $I_i(28)$[9] from the asymmetric unit as 'isostructural core' of 28 pairs of non-hydrogen atoms was computed. Percentages of 98.1 (**1/2**), 96.7 (**1/5**) and 95.5 (**2/5**) reveal high isostructurality (> 80 %) in the three molecular pairs as expected for isometric molecules differing in one substituent.[8] Even though the percentages are ordered as in the overlay diagrams, their variations are not consisting with those of the Π indices. These results prompted us to evaluate the effect combined of axial ratios and distance differences on the isostructurality by calculation of the *measure of similarity* Δ,[8] yielding values of 0.032 Å, 0.031 Å and 0.101 Å for **1/2**, **1/5** and **2/5** pairs, respectively.

Though these values reveal resemblance in the pairs **1/2** and **1/5** showing higher similarity when compared to **2/5**, which is consisting with the Π indices, the lightly highest similarity for the pair **1/5** is in contrast with the shortest unit-cell index of 0.010 for the pair **1/2.**

With the aim to compare the structures considering also the effect of neighboring molecules, we have calculated the *dissimilarity index* '*X*', and the group of twenty-seven atoms corresponding to the asymmetric unit was used to define the COSP.[9] The occurrence of 3D 'supramolecular constructs' in the crystal packing for the three complexes, and *X* values of 0.5, 1.1 and 1.4 for the **1/2**, **1/5** and **2/5** pairs, respectively, can be seen in Figs. S4-S6 (ESI†) and Table 5. *X* values indicate a high structural similarity for the **1/2** pair (X < 1.0), as well as moderate and close similarity for **1/5** and **2/5** pairs (1.0 < X < 6.0), in good agreement with the RMSD values, and the Π and $I_i(28)$ *indices*. Stretch parameter *D* in the range 0.07-0.29 Å (Table 5), as well as the *X*(i) vs. delta(d) and delta(p) vs. delta(a) plots (Figs. S4-S6, ESI†) reveal in general a small extent of stretching in one structure compared to the other. The overall results allow describing properly the isostructurality, and the formation of very similar packing motifs for the three complexes. The similarity of the powder XRD patterns (Fig. S7, ESI) and IR spectra (see analyses below in **3.3**) for complexes **1**, **2** and **5** is a result of this close structural relationship.

Based on the findings above, we have calculated *the dissimilarity index* for molecular pairs in two series of related compounds, namely M(1-Me_2p)$_2$[Fe(CN)$_5$NO] (M = Mn, Fe, Co, Ni, Zn, Cd)[13] and M(py)$_2$[Fe(CN)$_5$NO] (M = Mn, Co, Ni, Zn),[15] all the complexes being identified by its reference codes from CCDC. The result of calculations is shown in Table 5, revealing the occurrence of 3D supramolecular construct (isostructurality) in the crystal packing for all the fifteen pairs of complexes of the series with 1-methyl-2-pyrrolidone (1-Me2p) (Fig. S8, ESI†), and four pairs (OHIPED/OHIPON, OHIPIH/OHIPON, OHIPIH/OHIPUT and OHIPON/OHIPUT) of the series with pyridine (Py) (Fig. S9, ESI†).

The remaining two pairs exhibit 2D supramolecular construct (layer of molecules match), as well as moderate (X = 1.5) and low similarity (X = 6.5) for OHIPED/OHIPUT and OHIPED/OHIPIH, respectively. The pairs with 3D supramolecular construct present moderate isostructurality as reflected by the *dissimilarity index* in the ranges 2.2-5.6 and 1.1-5.7 for the series with pyrrolidone and pyridine, respectively.

In comparison to the **1/2**, **1/5** and **2/5** pairs, the structural dissimilarity is longer for the analogous pairs in the series with pyrrolidone, showing '*X*' values of 4.6, 2.2 and 5.4 for DOMCAM/DOMBUF, DOMCAM/DOMBEP and DOMBUF/DOMBEP pairs, respectively. In the series with pyridine a high similarity in the Co/Ni pair (X = 1.0) is observed,

View Article Online
DOI: 10.1039/D0CE01596B

Table 5. Space group (*SG*), lattice parameters (Å), formula units per cell (*Z*), *dissimilarity index* '*X*' and stretch parameter *D* (Å) for **1**, **2**, **5** and two series of related transition metal nitroprussides (CSD Refcodes)

	Mn	Fe	Co	Ni	Zn	Cd
			$M(1\text{-MeIm})_2[Fe(CN)_5NO]$			
	1	2	-	-	-	5
	SG				$P2_1/c$	
a	8.431(1)	8.386(2)	-	-	-	8.4002(3)
b	14.936(2)	14.787(4)	-	-	-	15.2133(5)
c	14.634(2)	14.458(3)	-	-	-	14.8960(5)
Z	4	4	-	-	-	4
X, D	Fe: 0.5, 0.07	Cd: 1.4, 0.27	-	-	-	Mn: 1.1, 0.22
			$M(1\text{-me2p})_2[Fe(CN)_5NO]$			
Refcodes	DOMCAM	DOMBUF	DOMBIT	DOMCEQ	DOMCIU	DOMBEP
	SG				$P2_1/n$	
a	20.5102(9)	20.26995(3)	20.2602(4)	20.1567(4)	20.3508(2)	20.78471(2)
b	13.2037(6)	13.1544(2)	13.1257(3)	13.0678(4)	13.0834(2)	13.2890(9)
c	7.6285(2)	7.5469(5)	7.4738(7)	7.3930(2)	7.4799(8)	7.7169(4)
Z	4	4	4	4	4	4
X, D	Fe: 4.6, 0.10 Zn: 3.7, 0.15	Co: 5.2, 0.08 Cd: 5.4, 0.22 Zn: 4.8, 0.09	Ni: 7.2, 0.12 Mn: 3.2, 0.12 Cd: 3.3, 0.24	Fe: 7.0, 0.19 Mn: 7.1, 0.23 Cd: 7.4, 0.32	Co: 4.5, 0.08 Ni: 5.6, 0.14	Mn: 2.2, 0.12 Zn: 4.1, 0.24
			$M(py)_2[Fe(CN)_5NO]$			
Refcodes	OHIPED	-	OHIPIH	OHIPON	OHIPUT	-
	SG				Ic2m	
a	18.8853(8)	-	18.5937(6)	18.5406(7)	18.6603(8)	-
b	13.7804(7)	-	13.6289(5)	13.4979(6)	13.5515(7)	-
c	7.5862(3)	-	7.427(2)	7.3879(3)	7.5040(3)	-
Z	2	-	2	2	2	-
X, D	Zn: 1.5, 0.12 Co: 6.5, 0.22	-	Ni: 1.0, 0.08	Zn: 5.7, 0.14 Mn: 7.3, 0.25	Co: 5.1, 0.12	-

1-methyl-imidazole (1-MeIm); 1-methyl-2-pyrrolidone (1-m2p); pyridine (py)

which differs of the analogous pair in the series with pyrrolidone showing low similarity (*X* = 7.2). In contrast with the series **1**-**5**, the Zn(II) complex is isostructural to the remaining complexes in the two series of related compounds. These differences suggest that the organic ligand play an important role in the occurrence of isostructurality for this kind of complexes.

Characterization through XPS data

The curve-fitting results from C 1*s*, N 1s and M 2*p* high-resolution XPS spectra are illustrated in Fig. 5. The C 1s spectra for complexes **1** and **2** were fitted with a superposition of five bands plus one weak signal at ~291 eV, that corresponds to the $\pi \rightarrow \pi^*$ transition. For the Fe(II) complex (**2**), a broad shoulder was found at ~288 eV, that suggests a certain reactivity of the Fe(II) complex with external contaminants such as CO. The peak at 283.8 eV was assigned to the axial CN group, which remains unbounded. The CN bridges at the equatorial positions are donating electrons to the metal centers and, therefore the electron density over the C and N atoms acquired a certain positive character that is reflected in the binding energy value found at 284.1 eV for **1** and +0.1 for compounds **2** and **3**. The contribution of the 1-Methylmidazole ligand into the C 1s spectra was fitted with two curves, that were assigned to the carbon atoms from the imidazole ring ($C_3H_3N_2$) plus the CH_3 substituent bounded to the N atom. The N atom is subtracting the electrons towards it and therefore the binding energy recorded for the carbon atom in the substituent (CH_3-N) is shitted +0.5 eV regarding to the carbon atoms in the Imidazole ring (285.2 eV). The strong signal at 284.8 eV was ascribed to the adventitious carbon. The C 1s spectra recorded from the Cu(II) complex is broader (FWHM= +0.3 eV) compared to those recorded from the Mn(II) and Fe(II) complexes. That increase in FWHM may be related to formation of sub-species such as $Cu^{1+}CN$, which results from the reduction of Cu^{2+} under the X-ray beam.

The N 1s spectra recorded for the three complexes are shown in the Fig. 5. Like the C 1s spectral region, the curve-fitting of the N 1s, consider contributions from unbridged and bridged CN groups at 397.2 ±0.1 eV and 397.8 eV, respectively. The imidazole ring is formed with two types of N atoms, whose contributions appear overlapped as prominent shoulder on the higher binding energy side of the main peak formed by the CN groups. The pyridinic N-atom is found forming a bond with the outer metal, T = Mn(II), Fe(II) and Cu(II), while the second N-atom is bonded to a CH_3 group. As mentioned above, in terms of electronegativity, the electron density on the N_{ring}-T bond

View Article Online
DOI: 10.1039/D0CE01596B

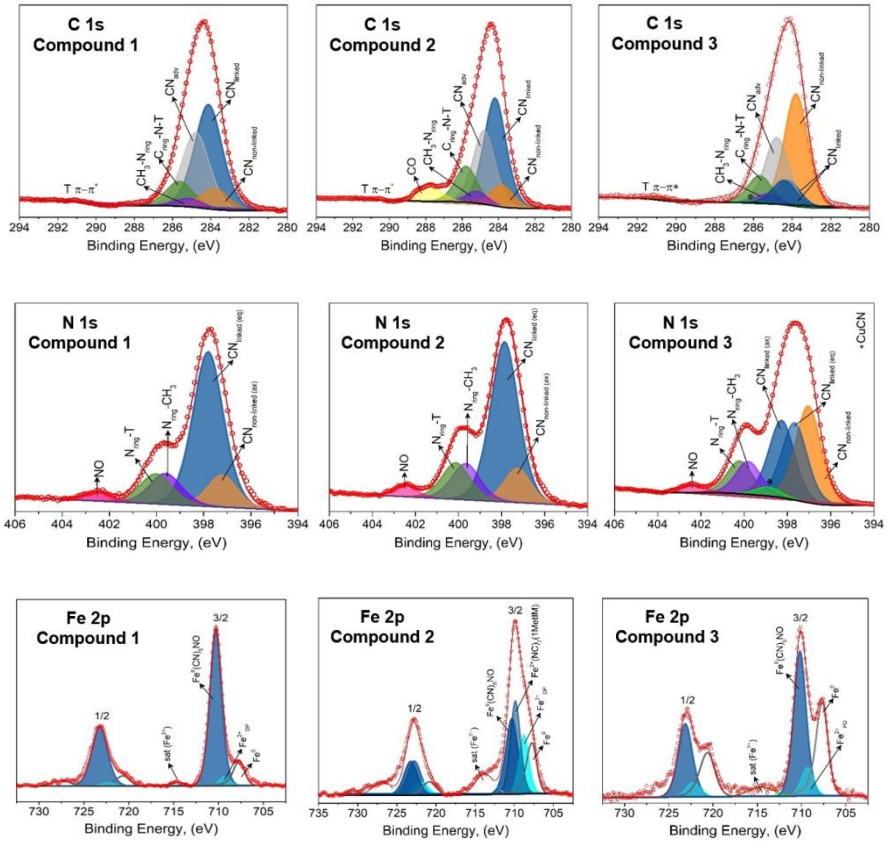

Fig. 5. Curve-fitting results from C 1s, N 1s and Fe 2p high-resolution XPS spectra of the complexes **1-3**. The blue and orange curves in C 1s and N 1s spectra correspond to the bonding nature of the CN groups. The green and purple curves represent the coordination of 1-methylimidazole (1-MeIm) in the complex. Sub-products of degradation (such as CuCN) resulting from the X-ray exposure during the XPS experiments are represent in C 1s and N 1s spectra with an asterisk (*) and in white and light blue curves for the Fe^0 species and Fe^{2+} (HS).

could show a more positive character regarding to N_{ring}-CH_3. In the region ~402.5 eV, a weak signal was assigned to the NO groups. Such high binding energy for the N-atom in the NO is related to its binding to the higher electronegative character for the oxygen atom. The N 1s spectrum recorded for **3** shows a main peak significantly broader compared to the spectra corresponding to the ones for compounds **1** and **2**. This is in accordance with the different coordination modes of the CN groups, where only one cyano group from the equatorial position is found forming a bond with the Cu(II) metal center. The last one is found forming a bond with the axial CN group. An additional signal was fitted at 398.9 eV, which corresponds to the CuCN.

The Fe atom in the nitroprusside ion is found with an oxidation state +2 in low-spin (LS) configuration, due to the strong character of the CN groups and the nitrosyl ligand. XPS is overly sensitive to this condition, and for that reason, the Fe 2p spectra for the nitroprusside ion (Fig. 5) is expected be represented by two symmetric narrow peaks (Fe $2p_{3/2}$-Fe $2p_{1/2}$) with a 3:2 intensity ratio. The experimental Fe spectra shown two additional peaks on the lower binding energy side assigned to Fe(II) in high-spin (HS) configuration, and Fe in metal state. The formation of both species is closely related with the exposure time to the X-ray beam during the experiment. Such effect remains documented from XPS spectra of sodium nitroprusside.[16a] This effect is more prominent in the sample of Cu(II) related to the trend of copper to reduce forming copper cyanide, and a similar behavior was previously reported and previously discussed.[16b] On the other hand, the Fe 2p spectra for the Fe(II) complex is composed of these two peaks plus the contribution from the Fe atom from the nitroprusside ion and the Fe acting as outer metal, where its coordination sphere is composed with two imidazole ligands plus four CN groups. In addition to the curve of Fe^{2+} in HS configuration (Fe_{DP}), the spectra showed a prominent shake-up satellite on the higher binding energy side of the main peak. Table S4-S7, ESI summarizes the binding energy values and parameters resulted from the curve-fitting processes. The Cu 2p and Mn 3s XPS spectra are shown in Figs. S21-S22, ESI.

DFT study

As commented above, the 2D polymers reported herein have a tendency to form, among others, lp–π and π–π stacking interaction in the solid state (see Figs. 1-3). This study focuses on the crucial influence of the intramolecular lp–π interaction between the nitrosyl ligand and the imidazole ring upon the π–

π stacking interaction. We have used a model of compound **4** as a representative compound exhibiting a combination of lp–π and π–π interaction that generates interesting lp–π/π–π/π–lp assemblies. In the model we have substituted the bridging CN ligands by monodentate HCN ligands with the intention to generate a monomeric model and to estimate the energy associated to the π-stacking interaction.

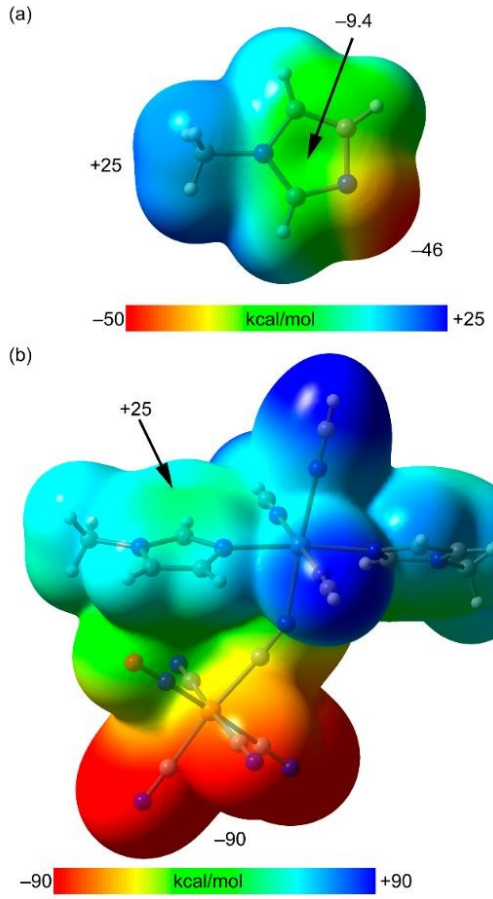

Fig. 6. (a) MEP surfaces of 1-methylimidazole, and (b) the theoretical model of **4**. The energies at selected points of the surfaces are indicated. Iso-surface 0.001 a.u.

First of all, we have computed the molecular electrostatic potential (MEP) surface of the 1-methylimidazole ligand and the theoretical model (see **Fig. 6a,b**). The most relevant issue is that the MEP over the center of the ring changes from negative in the free ligand (–9.4 kcal/mol) to large and positive (+24 kcal/mol) in the model of **4** due to the coordination to the Zn(II) metal center. The minimum MEP in the model of **4** is located at the CN ligands of the Fe(II) metal center.

We have studied the π–π stacking interaction in **4** using the dimers shown in Fig. 7. We have used three different dimers, one corresponds to the lp–π/π–π/π–lp assembly observed in the X-ray structure. In the second model, one nitroprusside fragment has been rotated in such a way that the intramolecular lp–π interaction is not formed (see small blue arrow in Fig. 7b). Finally, in the third model both nitroprusside fragments have been rotated (see Fig. 7c). It is interesting to note that the dimerization energy is moderately strong in the first model (ΔE_1 = –6.9 kcal/mol). Moreover, it is significantly reduced in the second model to ΔE_2 = –2.0 kcal/mol and, remarkably, is positive (ΔE_3 = +2.6 kcal/mol) in the third model where the lp–π interactions are absent. This result strongly suggests that the existence of the lp–π interaction at one side of the ring is necessary for the formation of the π-stacking interaction, indicating a strong cooperativity effect. This is likely due to the fact that the existence of the lp–π reduces the excess of positive charge over the aromatic ring, reducing the electrostatic repulsion.

The NCIplot has been used to confirm the existence of both interactions (lp–π and π–π) in the dimer of compound **4** in combination to the QTAIM distribution of critical points and bond path that emerge upon dimerization. The lp–π interaction is characterized by a bond CP (red sphere) and bond path that connects the O-atom of nitrosyl to one C-atom of the aromatic ligand (see Fig. 8). Moreover, a bluish iso-surface is located between the O and C atoms, thus further supporting the existence and attractive nature of the interaction. The π–π interaction is characterized by a more extended and green iso-surface located between both aromatic rings, thus confirming its attractive nature. Moreover, the π-stacking interaction is characterized by the presence of two symmetrically equivalent bond CPs that interconnect the N and C atoms of both rings. In addition, several ring and cage CPs also emerge upon complexation due to the formation of several supramolecular rings and cages.

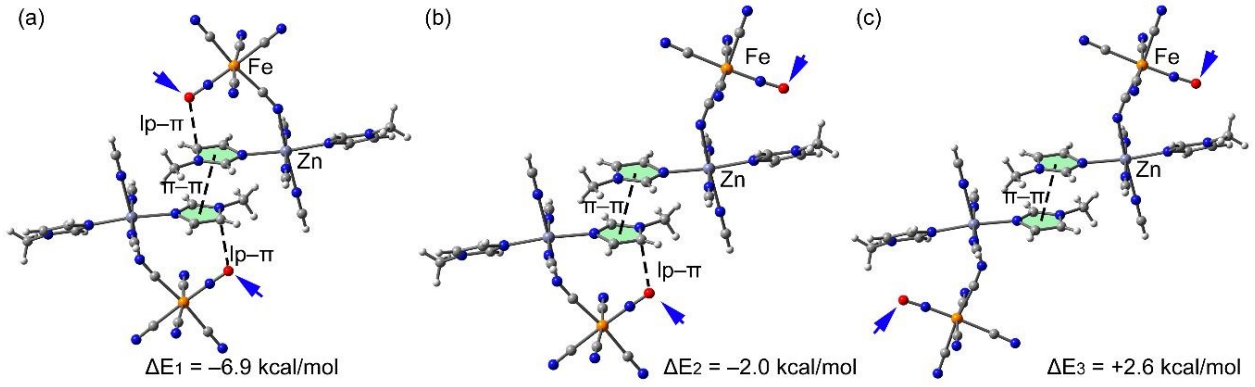

Fig. 7. Theoretical models used to analyze the π–π stacking interactions in **4**. (a) Models of the X-ray structure. (b) one nitroprusside unit is rotated with respect to the X-ray

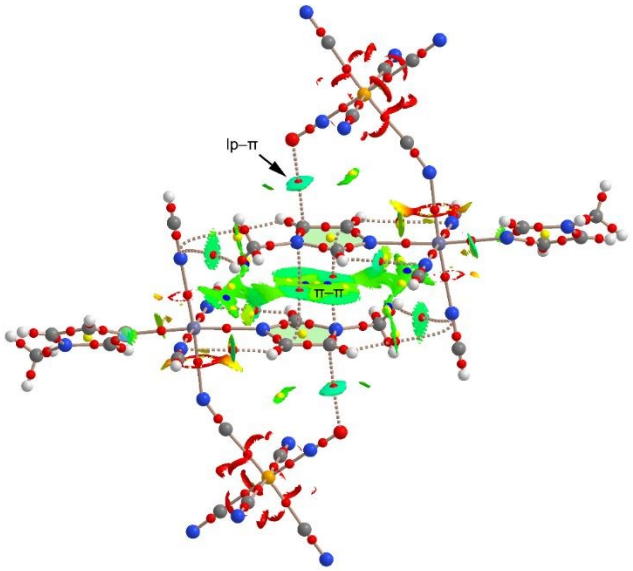

Fig. 8. QTAIM distribution or bond, ring and cage CPs (red, yellow and blue spheres, respectively) and bond paths for the theoretical dimer of compound **4**. The NCIplot surface is also indicated using an iso-surface of 0.5 a.u. and a –0.03 < ρ < 0.03 a.u. density range.

Magnetic properties

In the compounds under study, two types of magnetic interactions are possible between the metal centers M = Mn^{2+}, Fe^{2+}, Cu^{2+}. The Fe(II) ion in the nitroprusside moiety remains in the low spin (LS) state indicating its closed-shell nature. Generally, the distance between the M(II) metal centers in the chain ···M-N≡C-Fe-C≡N-M··· are above 10 Å and the magnetic interaction between the metal centers are antiferromagnetic in nature. A ferromagnetic interaction could be expected when the overlapping of the π clouds of the imidazole rings in the interlayer region is strong.

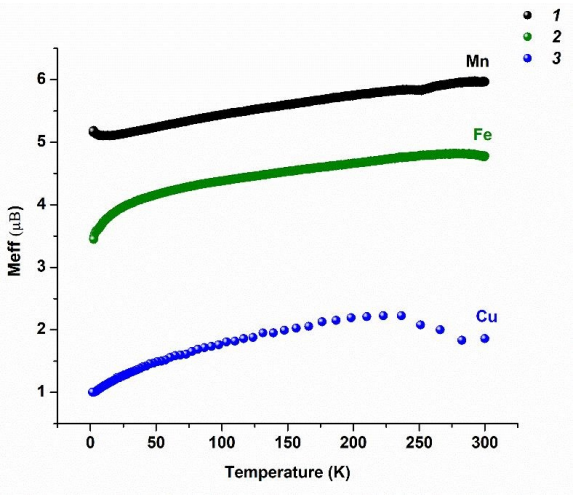

Fig. 9. Temperature dependence of effective magnetic moment (M_{eff}) measured in the applied field of 50 Oe for compounds **1-3**.

This behavior was observed in different inorganic-organic hybrid materials with imidazole and pyridine derivatives as intercalated ligands.[12-18] In this work, we have measured ZFC and FC curves to identify the possible magnetic interactions between metal centers from neighboring layers.

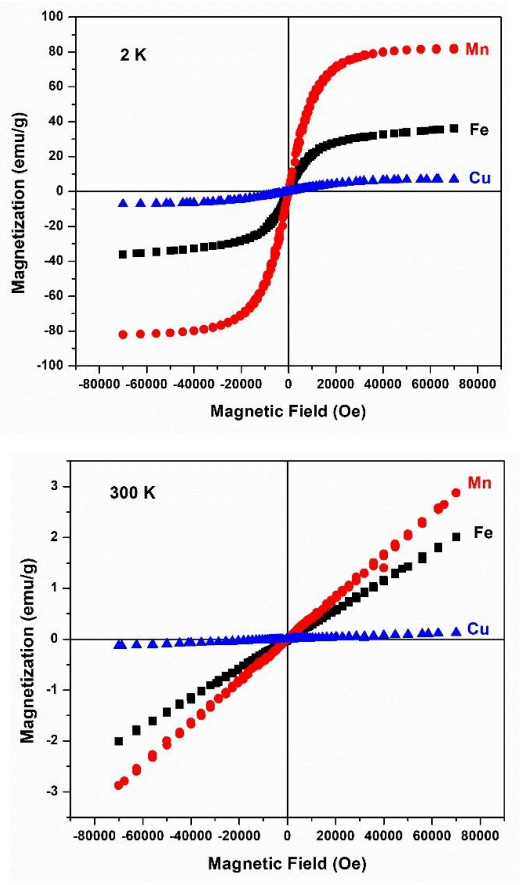

Fig. 10. Magnetization versus magnetic field for compounds **1-3** at 2 K (top) and 300 K (bottom).

Fig. 9 shows the temperature dependence of the effective magnetic moment (M_{eff}) for compounds **1** (Mn), **2** (Fe) and **3** (Cu), from the experimental magnetic data. The metal ions Mn(II), Fe(II) and Cu(II) in compounds **1**, **2** and **3**, respectively have unpaired electrons, and the samples remain in a paramagnetic state in all the temperature range, with weak antiferromagnetic coupling between the M(II) centers within the ···M-N≡C-Fe-C≡N-M··· chain. This behavior is more pronounced at low temperatures, as shown in Fig. 9, depicted by the decreasing curves. In these complexes, the overlap between π clouds of 1-MeIm molecules in neighboring layers is not strong and the interaction between M(II) ions in different layers is not possible. Compounds **1-3** are paramagnetic at room temperature, as evident from the linear curve of Magnetization versus applied magnetic field at 300 K (**Fig. 10**) without any hysteresis at 2 and 300 K.

Compounds **1**, **2** and **3** show effective magnetic moments of 5.96, 4.70 and 1.86 BM, respectively, at 300 K. These values are in accordance with the expected ones for a spin only contribution from a paramagnetic center in an isotropic octahedral environment (Mn: 5.92 BM, Fe: 4.90 BM and Cu: 1.73 BM).

The plot of 1/χ versus T (**Fig. S23, ESI**) is nearly linear in the range 2-300 K for complexes 1-3 indicating that the plots follow a Curie-Weiss law. The Curie-Weiss constants (θ_{cw}) are negative [-10.73, -20.41 and -16.64 K for **1**, **2** and **3**, respectively] suggesting weak antiferromagnetic coupling between M(II) ions, at very low temperatures.

Concluding Remarks

Five new polymeric transition M(II) metal (M = Mn, Fe, Cu, Zn, Cd) nitroprussides with 1-methylimidazole (1-MeIm), namely **1**-**5**, have been synthesized and characterized by IR, XPS and UV-Vis spectroscopy, thermal analysis, and structural single-crystal (**1** and **3**-**5**) and powder (**2**) X-ray diffraction. The supramolecular architecture of all the five complexes is stabilized by non-classical C-H···N hydrogen bonds and moderate lp(O)···π interactions, whereas the compounds **1**, **2**, **4** and **5** also exhibit O···N chalcogen and π-stacking interactions. An exhaustive analysis of four geometric descriptors allowed quantifying the structural similarity/dissimilarity in complexes **1**, **2** and **5**. The *dissimilarity index X* for molecular pairs **1**/**2**, **1**/**5** and **2**/**5** revealed high isostructurality with the occurrence of supramolecular construct SC A: 3D for the former (*X* = 0.5), and moderate for the other two pairs with *X* values of 1.1 and 1.4, respectively. The *index X* was also calculated in twenty-one pairs from two series of related compounds, indicating high isostructurality (*X* = 1.0) only in one pair, moderate (*X* = 1.5-5.7) in fourteen pairs, and becoming low (*X* = 6.5-7.4) in six pairs. The obtained results suggest that the nature of the organic ligand plays a relevant role, in addition to the central metal ion, on the structural similarity of complexes in transition metal nitroprussides. In accordance with the crystal data, the intermolecular interactions that stabilize the interlayer region are not strong enough to support a cooperative long range magnetic order through intermolecular contacts as a super exchange path. Magnetic studies indicate that complexes **1**-**3** show antiferromagnetic interactions at very low temperatures between adjacent M(II) metal centers based on negative Curie-Weiss constants (θ_{cw}= -10.73, -20.41 and -16.64 K obtained for complexes **1**, **2** and **3**, respectively). Finally, the DFT study reveals that the π-stacking interactions observed in the solid state of the compounds are strongly influenced by the O···π interactions involving the 1-methylimidazole and the nitrosyl ligand.

Conflicts of interest

There are no conflicts to declare.

Acknowledgments

DMG and ADS thank to ANPCyT (PICT 2016-0226) and SCAIT-UNT (Project 683), AF to MICIU/AEI, grant number CTQ2017-85821-R, FEDER funds, and GAE and OEP to CONICET (PIP 11220130100651CO) and UNLP (Grants to Projects 11/X709 and 11/X857) for financial support. Authors thank Dr. Edilso Reguera (CICATA-IPN) for XPS and magnetic measurements.

Notes and references

1 *(a)* B. Chen, L. Wang, Y. Xiao, F.R. Fronczek, M. Xue, Y. Cui and G. Qian, *Angew. Chem., Int. Ed*. 2009, **48**, 500-503; *(b)* C. S. K. Mak, D. Pentlehner, M. Stich, O. S. Wolfbeis, W. Chan and H. Yersin, *Chem. Mater*. 2009, **21**, 2173-2175; *(c)* M. L. Foo, R. Matsuda and S. Kitagawa, *Chem. Mater*. 2014, **26**, 310-322; *(d)* K. Boukheddaden, M.H. Ritti, G. Bouchez, M. Sy, M.M. Dirtu, M. Parlier, J. Linares and Y. Garcia, *J. Phys. Chem*. 2018, **122C**, 7597-7604.

2 *(a)* J. Lee, O. K. Farha, J. Roberts, A. Scheidt, S. T. Nguyen and J. T. Hupp, *Chem. Soc. Rev*. 2009, **38**, 1450-1459; *(b)* U. Diaz and A. Corma, *Chem. Eur. J*. 2018, 3944-3958; *(c)* L. Ma, C. Abney and W. Lin, *Chem. Soc. Rev*. 2009, **38**, 1248-1256.

3 *(a)* J. Werner, Z. Tomkowicz, M. Rams, S. G. Ebbingaus, T. Newmann and C. Näther, *Dalton Trans*. 2015, **44**, 14149-14158; *(b)* D. Nafday, D. Sen, N. Kaushal, A. Mukherjee and T. Saha-Dasgupta, *Phys. Rev. Research*, 2019, **1**, 032034; *(c)* J. Wu, N. Akhtar, T. T. M. Palstra and P. Rudolf, *J. Mater. Chem. C* 2017, **5**, 1782-1788.

4 *(a)* Y. Cui, G. Qian, J. Gao, L. Chen, Z. Wang, M. Wang, *J. Phys. Chem. B*, 2005, **109**, 23295-23299; *(b)* P. Matozzo, A. Colombo, C. Dragonetti, S. Righetto, D. Roberto, P. Biagini, S. Fantacci, D. Marinotto, *Inorganics*, 2020, **8**, 25.

5 Y. Shen, G. Cosquer, H. Ito, D. C. Izuogu, A. J. W. Thom, T. Ina, T. Uruga, T. Yoshida, S. Takaishi, B.K. Breedlove, Z. Y. Li and M. Yamashita, *Angew. Chem. Int. Ed*. 2020, **132**, 2420-2427.

6 Y. Lu, W. Xu, K. Hu, S. Jin, L. Sun, B. Liu and D. Wang, *Polyhedron*, 2019, **159**, 408-425.

7 A. I. Kitaigorodski, Molecular Crystals and Molecules, vol. 29 of Physical Chemistry, p. 74. New York and London, Academic Press, 1973.

8 J. Lima-de-Faria, E. Hellner, F. Liebau, E. Makovicky and J. E. Parthé, *Acta Crystallogr.,* 1990, **A46**, 1-11.

9 A. Kálmán, L. Párnkányi and G. Argay, *Acta Crystallogr*., 1993, **B49**, 1039-1049.

10 G. Bergerhoff, M. Berndt, K. Brandenburg, and T. Degen, *Acta Crystallogr.*, 1999, **B55**, 14 7-156.

11 (*a*) T. Gelbrich and M. B. Hursthouse, *CrystEngComm*, 2005, 7, 324-336; (*b*) T. Gelbrich and M. B. Hursthouse, *CrystEngComm*, 2006, **8**, 448-460; (*c*) F. P. A. Fabbiani, B. Dittrich, A. J. Florence, T. Gelbrich, M. B. Hursthouse, W. F. Kuhs, N. Shankland, and H. Sowa, *CrystEngComm*, 2009, **11**, 1396-1406; (*d*) T. Gelbrich, T. L. Threlfall and M. B. Hursthouse, *CrystEngComm*, 2012, **14**, 5454-544.

12 *(a)* D.M. Gil, H. Osiry, A. Rodriguez, A. A. Lemus-Santana, R.E. Carbonio and E. Reguera, *Eur. J. Inorg. Chem*. 2016, 1690-1696; *(b)* H. Osiry, A. Cano, A.A. Lemus-Santana, A. Rodríguez, R.E. Carbonio, E. Reguera, *J. Solid State Chem*. 2015, **230**, 374-380.

13 Y. Avila, H. Osiry, Y. Plasencia, A.E. Torres, M. González, A.A. Lemis-Santana, E. Reguera, *Chem. Eur. J*. 2019, **25**, 11327-11336.

14 A. Di Santo, H. Osiry, E. Reguera, P. Alborés, R.E. Carbonio, A. Ben Altabef, D.M. Gil, *New J. Chem*. 2018, **42**, 1347-1355.

15 Y. Avila, H. Osiry, A.E. Torres, L. Martinez-dlCruz, M. González, J. Rodríguez-Hernández, E. Reguera, J. Coord. Chem. 2020, 73, 347-359.

16 *(a)* A. Cano, L. Lartundo-Rojas, A. Schchukarev and E. Reguera, *New J. Chem*., 2019, **43**, 48, 4835-4848 ; *(b)* A. Cano, J. Rodríguez-Hernández, A. Shchukarev, E. Reguera, *J. Solid State Chem*. 2019, **273**, 1-10.

17 Y. Avila, Y. Plasencia, H. Osiry, L. Martínez-dlCruz, M. González, E. Reguera, *Eur. J. Inorg. Chem*. 2019, 4966-4973.

View Article Online
DOI: 10.1039/D0CE01596B

18 Y. Avila, P.M. Crespo, Y. Plasencia, H.R. Mojica, J. Rodríguez-Hernández, E. Reguera, *J. Solid State Chem*. 2020, **286**, 121293.
19 CrysAlisPro, Oxford Diffraction Ltd., version 1.171.33.48 (release 15-09-2009 CrysAlis171.NET).
20 G. M. Sheldrick, *Acta Cryst*. 2015, **A71**, 3–8.
21 G. M. Sheldrick, *Acta Cryst*. 2008, **A64**, 112-122.
22 O. V. Dolomanov, L. J. Bourhis, R. J. Gildea, J. A. K. Howard, H. Puschmann, *J. Appl. Crystallogr*., 2009, **42**, 339-341.
23 J. Rodríguez-Carvajal, *Physica B: Condensed Matter* 1993, **192**, 55-69.
24 A. Le Bail, *Powder Diffraction* 2005, **20**, 316-326.
25 C. F. Macrae, I. J. Bruno, J. A. Chisholm, P. R. Edgington, P. McCabe, E. Pidcock, L. Rodriguez-Monge, R. Taylor, J. van de Streek and P. A. Wood, *J. Appl. Crystallogr.*, 2008, 41, 466-470.
26 C. Adamo and V. Barone, *J. Chem. Phys.* 1999, *110*, 6158–6169.
27 S. Grimme, J. Antony, S. Ehrlich, H.A. Krieg, *J. Chem. Phys*. 2010, **132**, 154104
28 F. Weigend and R. Ahlrichs, *Phys. Chem. Chem. Phys*. 2005, **7**, 3297–3305.
29 M.J. Frisch, G.W. Trucks, H.B. Schlegel, G.E. Scuseria, M.A. Robb, J.R. Cheeseman, G. Scalmani, V. Barone, G.A. Petersson, H. Nakatsuji et al. Revision B.01; Gaussian, Inc.: Wallingford, CT, USA, 2016.
30 J. Contreras-García, E. R. Johnson, S. Keinan, R. Chaudret, J.-P. Piquemal, D. N. Beratan and W. J. Yang, *J. Chem. Theory Comput.* 2011, **7**, 625–632.
31 AIMAll (Version 13.05.06); Todd, A., Keith, T.K., Eds.; Gristmill Software, Overland Park, KS, USA, 2013.
32 S. F. Boys and F. Bernardi, *Mol. Phys*. 1970, **19**, 553.
33 L.E. Zelenkov, D. M. Ivanov, E. K. Sadykov, N. A. Bokach, B. Galmés, A. Frontera and V. Yu. Kukushkin, *Cryst. Growth Des*. 2020, **20**, 6956–6965.
34 (a) S. Thakur, D. M. Gil, A. Frontera and S. Chattopadhyay, *Polyhedron* 2020, **187**, 114676; (b) M. Karmakar, A. Frontera, S. Chattopadhyay, T. J. Mooibroek and A. Bauzá, *Int. J. Mol. Sci.*, 2020, **21**, 7091; (c) C. Verdugo-Escamilla, C. Alarcón-Payer, A. Frontera, J. Acebedo-Martínez, A. Domínguez-Martín, J. Gómez-Morales 1and D. Choquesillo-Lazarte, *Crystals*, 2020, **10**, 1088
35 A. V. Rozhkov, I. V. Ananyev, R. M. Gomila, A. Frontera and V. Yu. Kukushkin, *Inorg. Chem*. 2020, **59**, 9308–9314.
36 *(a)* A. Gavezzotti, J. Phys. Chem. B 2003, **107**, 2344-2353; *(b)* A. Gavezzotti, J. Phys. Chem. B 2002, **106**, 4145-4154.
37 T. Steiner, *Angew. Chem. Int. Ed*., 2012, **41**, 48-76.
38 (*a*) R. Taylor and O. Kennard, *J. Am. Chem. Soc*, 1982, **104**, 5063-5070; (*b*) R. Taylor, *Cryst. Growth Des*., 2016, **16**, 4165-4168.
39 C. Janiak , *J. Chem. Soc*., *Dalton Trans*., 2000, 3885-3896.
40 M. Egli, S. Sarkhel, *Acc. Chem. Res*. 2007, **40**, 197-205.
41 S. R. Choudhury, P. Gamez, A. Robertazzi, C.Y. Chen, H.M. Lee, S. Mukhopadhyay, *Cryst. Growth Des*. 2008, **8**, 3773-3784.
42 T. J. Mooibroek, P. Gamez and J. Reedijk, *CrystEngComm*, 2008, **10**, 1501-1515.

View Article Online
DOI: 10.1039/D0CE01596B

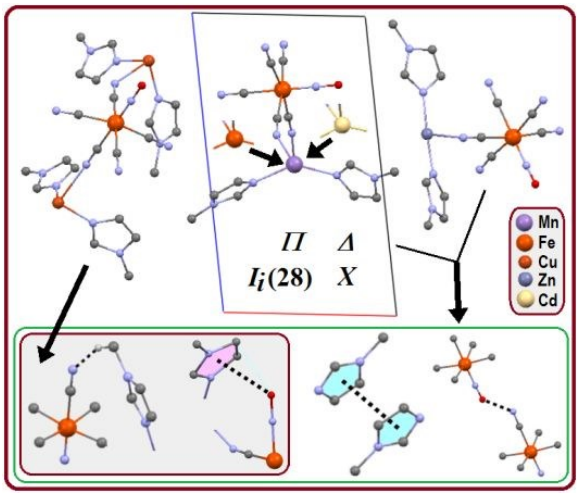

Transition metal M(II) (M = Mn, Fe, Cu, Zn, Cd) nitroprussides with 1-methyl-imidazole were prepared and characterized by spectroscopic techniques, thermal analysis, powder (Fe complex) and single-crystal XRD. H-bonds, N···O, π···π and lp(O)···π contacts control the crystal packing. Four geometric descriptors (Π, $I_i(n)$, Δ and X) were calculated for estimating isostructurality.